# Experimental determination of cross sections for $K$-shell ionization by electron impact for C, O, Al, Si, and Ti

Silvina P. Limandri,[1,2] M. A. Z. Vasconcellos,[3] Ruth Hinrichs,[4] and Jorge C. Trincavelli[2,5]

[1]*Centro Atómico Bariloche, Comisión Nacional de Energía Atómica, San Carlos de Bariloche (8400), Río Negro, Argentina*
[2]*Consejo Nacional de Investigaciones Científicas y Técnicas (CONICET), Argentina*
[3]*Instituto de Física, Universidade Federal do Rio Grande do Sul (UFRGS), Porto Alegre, Rio Grande do Sul, Brazil*
[4]*Instituto de Geociências, UFRGS, Porto Alegre, Rio Grande do Sul, Brazil*
[5]*Facultad de Matemática, Astronomía y Física, Universidad Nacional de Córdoba, Ciudad Universitaria (5000), Córdoba, Argentina*

(Received 6 June 2012; published 2 October 2012)

Cross sections for $K$-shell ionization by electron impact were determined from films of Al, Si, and Ti and their oxides deposited on carbon substrates, for incident energies between 2.5 and 25 keV. The spectral processing of the x-ray emission spectra took into account corrections due to the presence of a spontaneous oxide layer formed on the monoelemental films and to the supporting material. Carbon $K$-shell ionization cross sections were determined from the contribution of the substrate to the measured spectra, while for oxygen, data from the three oxide films were taken. The mass thickness of the coatings was characterized by x-ray reflectivity. The results obtained were compared with other experimental data sets, semiempirical approaches, and theoretical models.

DOI: 10.1103/PhysRevA.86.042701 PACS number(s): 34.80.−i, 32.80.Aa, 32.30.Rj, 02.70.Uu

## I. INTRODUCTION

It is important for basic and applied studies to comprehend the mechanism of $K$-shell vacancy creation by electron impact. Ionization cross sections must be known in order to properly describe the electron-matter interactions, e.g., to assess the radiation damage caused by the electron beam in medical applications. Accurate values of these ionization cross sections in a wide range of incident beam energies are necessary to perform standardless quantification by electron probe microanalysis (EPMA), Auger spectroscopy (AES), and electron energy loss spectroscopy (EELS). If the cross sections are known, elemental composition and thicknesses of stratified samples in EPMA [1] and trace elements in AES and EELS [2] can be determined.

A great number of theoretical approaches face the problem of predicting the $K$-shell ionization cross section $Q$. Each of these approaches has a certain range of validity in atomic number and incident beam energy. For example, the quantum formalism based on the relativistic plane-wave Born approximation (PWBA), developed in the framework of the conventional theory of stopping for high-energy particles [3], gives reliable values of $Q$ when the kinetic energy of the incident electron is higher than twenty times the critical energy of the shell to be ionized. The approximation worsens when the incident electron energy decreases, mainly because the theory neglects possible distortions of the projectile wave function due to the electrostatic field of the target atom. In the case of electronic collisions this approximation ignores interaction effects due to the indistinguishability between the projectile and the electrons belonging to the atom [4]. Better results are obtained by the relativistic distorted-wave Born approximation (DWBA), which includes distortion and exchange effects [4,5]. Ionization cross sections obtained by the DWBA theory involve the expansion of the incident electron wave function in series of partial waves regarding part of the interaction potential given by the electron-nucleus interaction [6]. Calculations based on this formalism are possible only for projectiles with low energies, because the convergence of the series degrades with increasing kinetic energy of the incident electron. Combined PWBA and DWBA approaches [4] produce reasonable values in a wide energy range. However, these calculations are difficult to implement, because they require long computing times and do not lead straightforwardly to analytical functions for $Q$. For these reasons, many empirical and semiempirical expressions for $Q$, useful to simulate x-ray emission spectra, can be found in the literature. Nevertheless, each of them only describes $Q$ in a restricted range of overvoltages $U$ (defined as the ratio between the incident beam energy and the ionization energy) and atomic numbers $Z$, reproducing the difficulties of the theoretical models. For instance, the expression of Green and Cosslett [7] is valid in the region $1 < U < 3$, while the one proposed by Quarles [8] is suitable for a wide range of $U$, but only for a few elements. The formula proposed by Hombourger [9] adequately describes the behavior of $Q$ in the range $1 < U < 20$ and $5 < Z < 79$. The analytical function fitted to theoretical data given by Campos *et al.* [10] is applicable in a larger range of $U$ for some atomic numbers.

The ionization cross section can be experimentally determined measuring the characteristic x-ray spectrum emitted by a thin sample of the specified element. The sample must be thin enough so that the incident electrons interact not more than once with the atoms of the film, rendering a characteristic x-ray intensity that is proportional to the ionization cross section. Self-supported films with nanometric thickness are difficult to produce, and usually the films have to be deposited on a substrate whose effects in the measured spectrum must be taken into account in the spectral processing. Several techniques can be used for film production: chemical vapor deposition, ion sputtering, electrochemical growth methods, etc.

In order to determine the precision of $Q$, the precision of all instrumental and atomic parameters that relate the x-ray characteristic intensity with the cross section have to be known. These include the film thickness and mass density, the intrinsic efficiency of the x-ray detector, the solid angle subtended by the detector, substrate effects, fluorescence yields, relative transition probabilities, and the mass concentration of the

 ©2012 American Physical Society

element of interest. The highest uncertainties are usually related to the determination of the film mass thickness [11]. The error in detector efficiency is also important [11], and affects mainly elements with low atomic number, whose characteristic energies are lower than 1 keV. Significant errors in the solid angle can arise from small modifications in the detector-sample distance or in the detector effective area. For these reasons and although ionization cross sections have been studied for a long time, the experimental data published by different authors disagree, with differences that sometimes are higher than the reported errors. A compilation of experimental values for $K$-shell ionization cross sections can be found in Refs. [12] and [13].

In this work, cross sections for $K$-shell ionization by electron impact were determined from the analysis of the x-ray emission spectra acquired at incident beam energies between 2.5 and 25 keV from Al, Si, and Ti films. In order to investigate a possible dependence of $Q$ with the oxidation state, also films composed by their oxides were analyzed, obtaining the oxygen ionization cross section as well. The carbon ionization cross section was calculated from the contribution of the substrates. X-ray emission spectra were processed with the software POEMA [14], including the effects due to the substrate and those caused by a spontaneous oxide layer grown on the monoelemental films. Thickness and density of the films were characterized by x-ray reflectivity (XRR). The results were compared with experimental data from other authors [11,15–22] and with theoretical and semiempirical curves available in the literature [4,9,10,23–28].

## II. EXPERIMENT

Each of the films enumerated in Table I was deposited simultaneously on two different substrates: a vitreous carbon planchet (Ted Pella) and a moncrystalline silicon (111) wafer, by means of ion magnetron sputtering with an ultrahigh vacuum equipment (AJA International ATC Orion 8). The base pressure in the deposition chamber was $3 \times 10^{-8}$ Torr and the sputtering pressures ranged between $2 \times 10^{-3}$ and $3 \times 10^{-3}$ Torr. All mass deposition rates were measured with a calibration crystal and converted to thickness using the nominal bulk density. Deposition rates and sputtering times are also listed in Table I.

The thickness and density measurements with XRR were performed on the films deposited on the silicon substrates, because they had larger areas than the carbon planchets. Cu-$K\alpha$ radiation was used in glancing angle Bragg-Brentano geometry in an x-ray diffractometer (Shimadzu XRD-6000). Two reflectivity patterns with a $2\theta$ angular step of 0.004° were acquired for each film: one in the $2\theta$ angular range between $-0.1°$ and 1.2°, with an acquisition time of 1 s per step and an Al filter, the other one in the angular range between 0.6° and 7°, with 2 s per step and without a filter. The first set of measurements was used to obtain the angular position $\theta_Z$ of the maximum reflected intensity to calibrate the position of the critical angle $\theta_c$. The second set contained the interference patterns of the x rays reflected inside the films that allowed the calculation of their thicknesses. The XRR patterns were processed with the software X'PERT REFLECTIVITY.

The x-ray emission spectra were measured on the films deposited on the carbon substrates (and on the pristine carbon planchet itself), taking advantage of the lower backscattering coefficient of carbon that causes less interference than silicon. The electron gun of a multibeam SEM-FIB (JEOL JIB-4500) was used to excite the spectra, which were acquired using an energy dispersive x-ray spectrometer (EDX) with a silicon drifted detector (SDD Thermo Scientific Ultradry). According to the supplier this detector has an effective area of 10 mm$^2$, a 300-nm polymer window, a 30-nm aluminum Ohmic contact, and a dead layer of 100 nm. The detector efficiency is reduced by a factor of 0.77 due to the shadowing of the grid that supports the ultrathin window. Measurements were performed with a 35° takeoff angle (18-mm working distance), 300-s live time, a sample-detector distance of 58 mm, and a specimen current of 4 nA. The incident beam current was measured with a Faraday cup. A list of the incident energies used can be found in Table I.

## III. METHODOLOGY

### A. Determination of thickness and density by XRR

The values of the thickness and density, necessary to obtain the cross sections, were determined with the aid of XRR patterns, that show a critical angle $\theta_C$ proportional to the mass density $\rho$, while the amplitude and periodicity of the oscillations give information about the linear thickness $x$ [29]. The critical angle was assumed as the angle at which the intensity fell to half of the maximum intensity. The linear thickness $x$ was calculated from the positions of the maxima and minima in the oscillation region. For each pair of consecutive maxima (or minima) a value of $x$ was obtained using the software X'Pert Reflectivity, and an average computed for each film. Additionally, the software calculated

TABLE I. Deposition rates and times used for film production and electron beam energies $E_o$ used to excite x-ray spectra.

| Film | Deposition rate (Å/s) | Time (s) | $E_o$ (keV) |
|---|---|---|---|
| Si | 0.3 | 333 | 2.5, 3, 4, 5, 7, 10, 15, 20 |
| $SiO_2$ | 0.2 | 580 | 2.5, 3, 4, 5, 7, 10, 15, 20 |
| Ti | 4.2 | 34 | 6, 7, 8, 9, 10, 12, 15, 20, 25 |
| $TiO_2$ | 0.09 | 1112 | 6, 7, 8, 9, 10, 12, 15, 20, 25 |
| Al | 4.5 | 34 | 2.5, 3, 4, 5, 7, 10, 15, 20 |
| $Al_2O_3$ | 0.08 | 1250 | 2.5, 3, 4, 5, 7, 10, 15, 20 |
| C substrate | | | 2.5, 3, 4, 5, 6, 7, 8, 9, 10, 12, 15, 20, 25 |

the Fourier transform of the reflectivity patterns, that, when resulting in a peaked curve, allowed us to estimate a mean thickness.

### B. Spectral processing

X-ray emission spectra were processed with the software POEMA [15], whose main features are described in this subsection and in Sec. III C. This program minimizes the quadratic differences between the experimental spectrum and an analytical function proposed to describe it. This function includes the background, the characteristic peaks, detection artifacts and, particularly, the effect of a native oxidation layer with adjustable thickness.

The expression used by POEMA to predict the number of photons $I_i'$ in the energy interval $[E_i, E_i + \Delta E]$ associated with the energy $E_i$ of the $i$th channel is

$$I_i' = \left[ B(E_i) + \sum_j P_j H_j(E_i) + P_{\mathrm{Ox}} H_{\mathrm{Ox}}(E_i) + P_{\mathrm{subs}} H_{\mathrm{subs}}(E_i) + I_{sp}' H_{sp}(E_i) \right] \Delta E, \quad (1)$$

where $B(E_i)$ is the function that describes the bremsstrahlung [30], $P$ is the peak intensity of a characteristic $K$ line, $H(E_i)$ accounts for the peak shape function [31], the subindices $j$, Ox, and subs refer to the elements that compose the films, the oxide layer, and the carbon substrate, respectively. $I_{sp}'$ denotes the contribution of spurious radiation (carbon sum peak, escape peaks, and the internal fluorescence peak of the detector) and $\Delta E$ is the channel width. The global parameters refined by POEMA are the scale factor involved in the bremsstrahlung prediction, the peak scale factor, the spectrometer gain and zero, the parameters related to peak widths, and the spontaneous oxide layer thickness. Individual peak parameters can be also optimized by the program, such as asymmetry coefficients, elemental concentrations, and relative transition probabilities.

The refinement procedure must be carried out through a cautious sequence of minimization steps in order to get the best fit of the experimental spectrum. In addition, the physical validity of results obtained in each step must be evaluated to avoid local minima in the function to be minimized.

The intensity $P_j$ of a characteristic $K$ line of the element $j$ in a film with mass thickness $(\rho x)_{\mathrm{film}}$ deposited on a carbon substrate can be written as [32]

$$P_j = \alpha \varepsilon C_j \, (\rho x)_{\mathrm{film}} \frac{N_A}{A_j} \omega_j f \Phi_{\mathrm{oC}} Q_j, \quad (2)$$

where $\alpha$ is the adjustable peak scale factor, $\varepsilon$ is the intrinsic efficiency of the detector, $N_A$ is Avogadro's number, and $f$ is the relative transition probability of the considered line. The factors $C_j$, $A_j$, $Q_j$, and $\omega_j$ are, respectively, the mass concentration, the atomic weight, the $K$-shell ionization cross section, and the fluorescence yield, from element $j$. The analytical function used to describe the ionization cross section [10] and other parameters involved in the prediction of characteristic intensities are discussed elsewhere [33].

The surface ionization $\Phi_{\mathrm{oC}}$, which includes the effect that electrons backscattered in the substrate ionize the film, can be expressed as

$$\Phi_{\mathrm{oC}} = 1 + 2\eta_{\mathrm{C}} f_{N\,\mathrm{film}}, \quad (3)$$

where $f_{N\,\mathrm{film}}$ is the fraction of electrons arriving at the substrate [32] and $\eta_{\mathrm{C}}$ is the backscattered electron coefficient for carbon. Equation (2) is valid for thin films where the incident electrons interact not more than once. To minimize the influence of the backscattered electrons from the substrate, a supporting material with low $\eta$ should be used, making carbon a convenient choice.

The strategy for the spectral fitting was to refine the global parameters in a wide spectral region including all the characteristic peaks and then to refine the background scale factor and the $\alpha$ parameter in a region of 500 eV around each characteristic peak. Even though the results were obtained by fitting the overall spectrum, the ionization cross sections mainly depend on the information contained in a narrow spectral region around the $K\alpha$ peak of the considered element.

The ionization cross sections presented here are averages from (i) the six films and the pristine substrate in the case of carbon; (ii) the three oxide films for oxygen; (iii) Al and $Al_2O_3$ for aluminum; (iv) Si and $SiO_2$ for silicon; and (v) Ti and $TiO_2$ for titanium. The mean values were obtained by weighting the experimental data with the inverse of the corresponding uncertainties.

### C. The oxidation layer and the carbon sum peak

A spontaneous oxide layer on the elemental film surfaces was detected with the high-sensitivity SDD detector with an ultrathin window. Even though this oxide layer is very thin (usually around a few nanometers) and has been disregarded in the older literature [11], it does influence the x-ray spectra measured at low voltages, as can be observed in the spectra of the carbon substrate and of the aluminum film measured at 3 keV (Fig. 1). Both spectra present a peak approximately at 0.5 keV. In the carbon spectrum this is the carbon sum peak. In the aluminum spectrum the peak at the same energy is much higher and is partially due to O-$K$ emission. Note that this film is nominally metallic aluminum, deposited in ultrahigh vacuum.

The contribution to the O-$K$ intensity $P_{\mathrm{Ox}}$ due to the spontaneous oxide layer in the Al, Si, and Ti films can be expressed as

$$P_{\mathrm{Ox}} = \alpha \varepsilon C_{\mathrm{O}} \, (\rho x)_{\mathrm{Ox}} \frac{N_A}{A_{\mathrm{O}}} \omega_{\mathrm{O}} \Phi_{\mathrm{oC}} Q_{\mathrm{O}}, \quad (4)$$

where $(\rho x)_{\mathrm{Ox}}$ is the mass thickness of the oxide layer, the subindex O refers to oxygen, and the other parameters are analogous to Eq. (2).

To deal with the problem that the carbon sum peak overlaps with the oxygen $K$ line, special attention had to be paid to determine the oxygen $K$-shell ionization cross section in the oxide films and to estimate the thickness of the spontaneous oxide layer on the monoelemental films. To determine the mean energy of the carbon sum peak and to find the correlation between its intensity and the C-$K$ intensity, spectra from the pristine carbon planchet measured at several incident energies

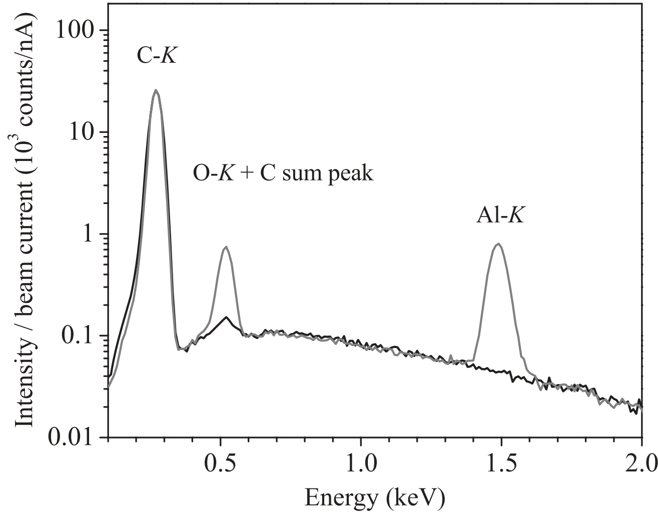


FIG. 1. Spectrum of Al film deposited on carbon substrate (gray line) and of carbon substrate itself (black line) measured at 3 keV, showing the presence of a spontaneous oxide layer grown on the sample surface.

were used (Table I). Using the nominal calibration parameters (spectrometer gain and zero), the mean energy of the carbon sum peak was 0.54 ± 0.01 keV, which is slightly different from the double of the C-$K$ energy value published by Bearden (i.e., 0.554 keV) [34].This small difference can be attributed to nonlinear calibration and electronic noise of the preamplifier that deteriorates the pile-up rejection efficiency for energies next to C-$K$ [35]. In addition, the energy of the sum peak depends on the degree of overlap between the signals entering the detector [36]: The smaller the temporal overlap, the lesser the energy of the resulting sum peak. According to Knoll [36], there should be a linear relationship with null intercept between the sum peak intensity and the square of the C-$K$ line. The linear behavior was corroborated by our results; however, the linear fit had a nonzero intercept (Fig. 2). These fit parameters

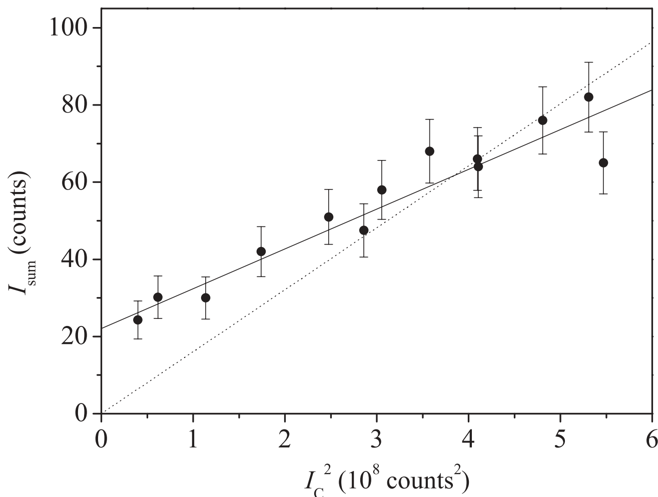


FIG. 2. Intensity of the carbon sum peak $I_{\mathrm{sum}}$ as function of the square of the C-$K\alpha$ peak intensity. Linear fit with nonzero (solid line) and null (dotted line) intercept.

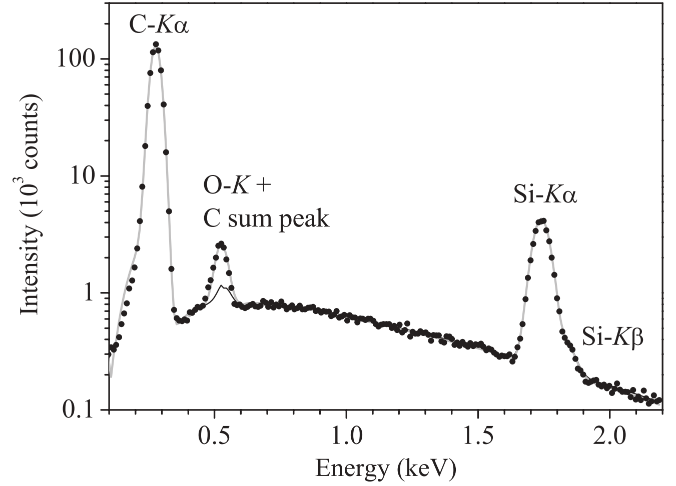


FIG. 3. X-ray emission spectrum from Si film, measured at 3 keV. Dots: experimental data; gray line: fit considering substrate and oxide layer effects; black line: fit considering only substrate effects.

were included in the program POEMA to account for the carbon sum peak.

Figure 3 shows the improvement of the fit when the thin oxide layer on the Si film is considered. The mass thickness obtained for the oxide layer on the silicon sample was 0.061 ± 0.002 $\mu$g/cm$^2$, which corresponds to a linear thickness of 2.3 ± 0.1 nm using a bulk density of 2.64 g/cm$^3$ for $SiO_2$. On the Al film the oxide layer had a mass thickness of 0.21 ± 0.08 $\mu$g/cm$^2$, corresponding to a linear thickness of 5.4 ± 0.2 nm (bulk density of 3.97 g/cm$^3$). The estimation of the oxide layer thickness on the Ti film was not possible, because the Ti $L$ lines overlap strongly with the O-$K\alpha$ line. In the refinement procedure, the thickness of the titanium oxide layer was arbitrarily stipulated as being 2 nm, slightly thinner than the native oxide on the silicon sample. This resulted in a mass thickness of 0.085 $\mu$g/cm$^2$, taking the bulk density of titanium oxide as 4.26 g/cm$^3$. The Ti-$L$ line energies used in the refinement are according to Bearden [34] and the relative transition probabilities were extrapolated from the data of Pia *et al.* [37].

### D. The solid angle subtended by the detector

The $\alpha$ parameter [Eqs. (2) and (4)] was obtained from the experimental spectra for each element in the sample and for each incident energy. Assuming that all the factors in Eq. (2) are accurately known, the $\alpha$ values should be equal to the product of the beam current, the acquisition live time, and the solid angle subtended by the detector. The ratio between $\alpha$ and this product was associated with a correction $\xi_Q$ to the ionization cross section used by the fitting program:

$$\xi_Q = \alpha \left( i\,\Delta t \frac{\Delta\Omega}{4\pi} \right)^{-1}. \tag{5}$$

Therefore, the ionization cross section obtained in this work is the product $\xi_Q Q$. It should be noted that the cross section determined by this method does not depend on the performance of the model of ionization cross section implemented in the fitting program, but depends on the accuracy level of the solid

angle subtended by the detector and the parameters involved in Eqs. (2) and (4).

To determine the solid angle subtended by the x-ray detector, the bremsstrahlung generated between 3 and 6 keV by a carbon substrate when irradiated with 15-keV electrons was simulated with the PENCYL subroutine of the PENELOPE software [38].

Let $b(E, \Delta E_{\text{sim}}, E_{\text{o}}, \Delta\Omega_{\text{sim}})$ be the value resulting from the simulation for the number of bremsstrahlung photons per incident electron, per energy interval $\Delta E_{\text{sim}}$ that emerges from the sample with energies between $E$ and $E + \Delta E_{\text{sim}}$ at a takeoff angle $\theta_{\text{TOFF}}$ in the solid angle $\Delta\Omega_{\text{sim}}$ for an incidence energy $E_{\text{o}}$. The relation between the measured bremsstrahlung intensity $I(E)$ in the energy range between $E$ and $E + \Delta E$ per energy interval and $b(E, \Delta E_{\text{sim}}, E_{\text{o}}, \Delta\Omega_{\text{sim}})$ can be written as

$$I(E) = i\,\Delta t \frac{\Delta\Omega}{4\pi}\frac{1}{\Delta E}\varepsilon(E)\, b\,(E, \Delta E_{\text{sim}}, E_{\text{o}}, \Delta\Omega_{\text{sim}}) \times \Delta E_{\text{sim}} \left(\frac{\Delta\Omega_{\text{sim}}}{4\pi}\right)^{-1}, \quad (6)$$

where $i$ is the beam current, $\Delta t$ the acquisition live time, $\Delta\Omega$ is the experimental solid angle (to be determined), $\varepsilon(E)$ is the intrinsic efficiency of the detector at energy $E$, and $\Delta E$ is the channel width in the measured spectrum (spectrometer gain), with the same value as was used for $\Delta E_{\text{sim}}$.

By comparing the experimental spectrum $I(E)$ with the values of the Monte Carlo simulation, the solid angle can be determined, assuming that all other parameters are known. In this work, the simulation was performed for a carbon sample measured at 15 keV in the energy range of 3–6 keV, where the intrinsic efficiency of the detector is almost constant. To be able to simulate over a billion primary electron trajectories within an acceptable simulation time, the x-ray emission was integrated over all azimuthal angles. The results from the simulation were compared with the bremsstrahlung measurements.

### E. Estimation of uncertainties

It is necessary to know the degree of accuracy of all the parameters involved in Eq. (2) to be able to estimate the uncertainty of the ionization cross section $Q_j$. Summing the squares of the errors of each parameter, the following upper limit of the relative error of $Q_j$ is obtained:

$$\left(\frac{\Delta Q_j}{Q_j}\right)^2 = \left(\frac{\Delta C_j}{C_j}\right)^2 + \left(\frac{\Delta\Phi_{\text{oC}}}{\Phi_{\text{oC}}}\right)^2 + \left(\frac{\Delta f}{f}\right)^2 + \left(\frac{\Delta P_j}{P_j}\right)^2 + \left(\frac{\Delta\omega_j}{\omega_j}\right)^2 + \left(\frac{\Delta\rho_{\text{film}}}{\rho_{\text{film}}}\right)^2 + \left(\frac{\Delta x_{\text{film}}}{x_{\text{film}}}\right)^2 + \left(\frac{\Delta\varepsilon}{\varepsilon}\right)^2 + \left(\frac{\Delta i}{i}\right)^2 + \left(\frac{\Delta t}{t}\right)^2 + \left[\frac{\Delta(\Delta\Omega)}{\Delta\Omega}\right]^2, \quad (7)$$

where the last three terms on the right of Eq. (7) are the square of the relative error of the $\alpha$ parameter, appearing in Eq. (2).

The characteristic $K$-line intensities were measured with a statistical error lower than 1%. The error associated with the backscattered electrons from the carbon substrate (involved in the calculation of $\Phi_{\text{oC}}$), is negligible compared to the other sources of error. According to Perkins *et al.* [39] a reasonable value for the uncertainties of the fluorescence yields of carbon and oxygen is 15%, while for the $K$-shell the $\omega$ factor is known with a precision of around 10% for Al and Si and of 3% for Ti [40].

The error associated with the detector efficiency depends on the thickness of the internal layers (an uncertainty of 8% was assumed) and on their respective mass attenuation coefficients, for which the errors are given by Chantler [41]. The resulting detector efficiency uncertainties are around 10% in the energy range between the C-$K$ and O-$K$ lines. This deviation decreases with increasing photon energies, being around 1% for Al-$K\alpha$ and Si-$K\alpha$ and 0.2% for Ti-$K\alpha$. The beam current was determined with a fluctuation lower than 1% and the variation in the live acquisition time was even lower and was disregarded. The determination of the parameters $\Delta\Omega$ and $\rho x$ and their error estimates are discussed in the next subsections.

## IV. DETERMINATION OF MASS THICKNESS AND DETECTOR SOLID ANGLE

### A. Thickness and density results

The critical angle, the average values and standard deviations of the density obtained with XRR, the nominal density of bulk material, and the linear thickness (from XRR) are shown in Table II. When the Fourier transform (FT) of the reflectivity patterns showed a defined maximum, the linear thicknesses obtained with this method were also included.

Regarding the values obtained for the mass densities, it can be seen that, in all the cases, the density obtained from the critical angle is lower than the bulk value, as was reported by other authors for sputtered films [42]. The uncertainties of the mass densities were estimated assuming an error in the critical angle position equal to the angular step used in the acquisition of the XRR patterns, being less than 2% in all the cases. The relative uncertainties associated with the thickness $x$ are below 10% except for alumina, where it is the main source of error in the estimate of ionization cross sections.

### B. Estimation of the solid angle subtended by the x-ray detector

Using the information provided by the manufacturer, a detector with a nominal area of 10 mm$^2$ placed at a distance

TABLE II. XRR parameters: critical angle $\theta_C$; density $\rho(\theta_C)$; nominal bulk density $\rho_{\text{nominal}}$; thickness from oscillations: MinMax; thickness from Fourier transform: FT.

| Film | $\theta_C$ (degrees) | $\rho(\theta_C)$ (g/cm$^3$) | $\rho_{\text{nominal}}$ (g/cm$^3$) | Thickness $x$ (nm) MinMax | FT |
|---|---|---|---|---|---|
| Al | 0.2167 | 2.31 ± 0.02 | 2.7 | 11.3 ± 0.1 | [a] |
| $Al_2O_3$ | 0.2592 | 3.29 ± 0.05 | 3.97 | 12 ± 2 | 12 |
| Si | 0.2185 | 2.28 ± 0.04 | 2.32 | 12.8 ± 0.5 | 12.4 |
| $SiO_2$ | 0.2095 | 2.14 ± 0.04 | 2.64 | 12.7 ± 0.6 | [a] |
| Ti | 0.2669 | 3.86 ± 0.05 | 4.5 | 11 ± 1 | 10.7 |
| $TiO_2$ | 0.2661 | 3.56 ± 0.04 | 4.26 | 10.9 ± 0.8 | 10.2 |

[a]The Fourier transform in these cases had no clearly defined peak.

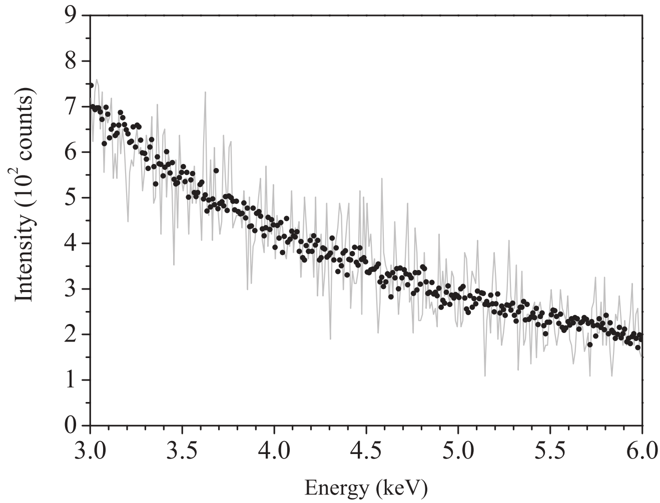


FIG. 4. Bremsstrahlung from the carbon bulk sample measured at 15 keV (dots) and simulated using the detector acceptance solid angle calculated in this work (line).

of 58 mm from the sample has a solid angle of $3.0 \times 10^{-3}$ sr. However, taking into account that the effective area of the detector is reduced due to the x-ray collimators in front of the ultrathin window, the solid angle may be much smaller. Variations of the sample-detector distance as well lead to modifications of the solid angle. For example, an error of 3 mm of the detector position will produce a 10% alteration of the solid angle.

As mentioned in Sec. III D, instead of using geometrical considerations based on nominal values, in this work, the strategy followed to determine the solid angle was to compare the experimental and the simulated bremsstrahlung. The mean solid angle obtained by this method was $(2.01 \pm 0.12) \times 10^{-3}$ sr, 30% lower than the value provided by the manufacturer. Figure 4 shows the experimental data and the spectrum calculated with the right-hand side of Eq. (6) using the value determined for $\Delta\Omega$ and the values of $b(E, \Delta E_{\rm sim}, E_{\rm o}, \Delta\Omega_{\rm sim})$ obtained from the simulation.

## V. RESULTS AND DISCUSSION

The results obtained for the $K$-shell ionization cross sections for C, O, Al, Si, and Ti are shown in Figs. 5–9 (circles), together with experimental (other symbols), theoretical, and semiempirical data (lines) obtained by other authors. The data for carbon are the averages from the six films and the pristine substrate (Fig. 5). The data for oxygen are averaged from the three oxide films (Fig. 6). The data for aluminum from Al and $Al_2O_3$ films are shown separately as filled and open circles (Fig. 7), analogously as the data for silicon (Fig. 8) and titanium (Fig. 9), where the ionization cross sections from the pure elements and the corresponding oxides are shown.

The theoretical curves shown in Figs. 5(b)–9(b) are based on PWBA from Barlett and Stelbovics [23] and have been improved at higher energies by Tiwari and Tomar [24]. The latter authors took into account exchange, Coulomb, and relativistic effects along with contributions due to transverse interaction of virtual photons, causing a general improvement but, however, overshooting the mean values at low energies. For C, O, and Al [Figs. 5(b)–7(b)] theoretical results given by Khare *et al.* [25] were plotted. These authors used PWBA including the acceleration suffered by the incident electron due to the electric field of the nucleus of the target atom. Calculations based on the relativistic version of the binary-encounter Bethe model (RBEB), published by Santos *et al.* [26] were also included.

Semiempirical expressions obtained by the fitting of experimental data performed by Hombourger [9] and the functions proposed by Haque *et al.* [27] and by Talukder *et al.* [28] were plotted in Figs. 5(b)–9(b). In these functions, the formula of Bell *et al.* [43] was used, including relativistic corrections and ionic effects as a basis for the fitting of experimental data. In order to assess the expressions proposed by these authors, the $K$-shell ionization absorption edges reported by Bearden and

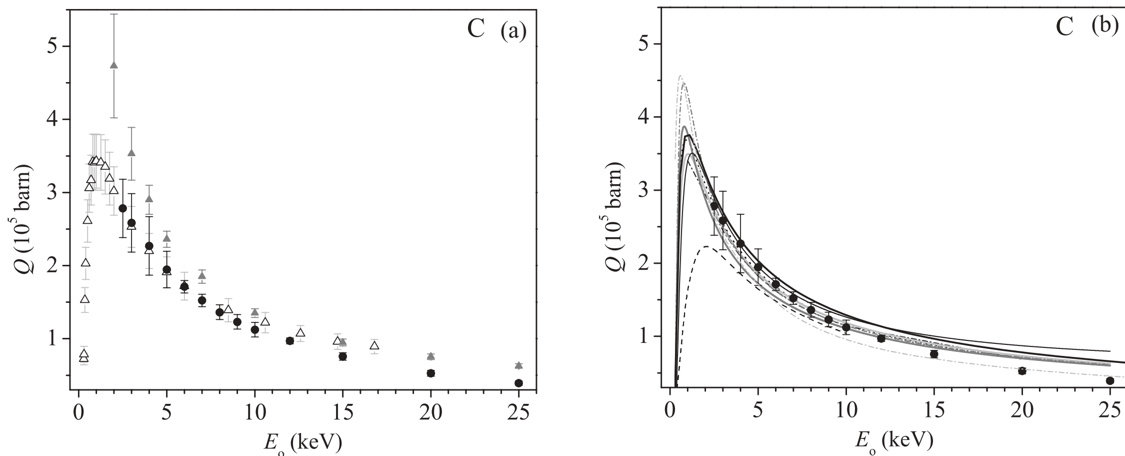


FIG. 5. Ionization cross section for carbon as a function of electron energy $E_{\rm o}$. (a) Comparison between experimental determinations. (b) Experimental data obtained in this work compared with theoretical and semiempirical approximations. Circles: this work; open triangles: Ref. [21]; solid triangles: Ref. [22]; black thin solid line: Ref. [4]; light gray thick solid line: Ref. [9]; black thick solid line: Ref. [10]; black dashed line: Ref. [23]; black dotted line: Ref. [24]; light gray dash dotted line: Ref. [25]; black dash dotted line: Ref. [26]; dark gray thick solid line: Ref. [27]; and dark gray dash dotted line: Ref. [28].

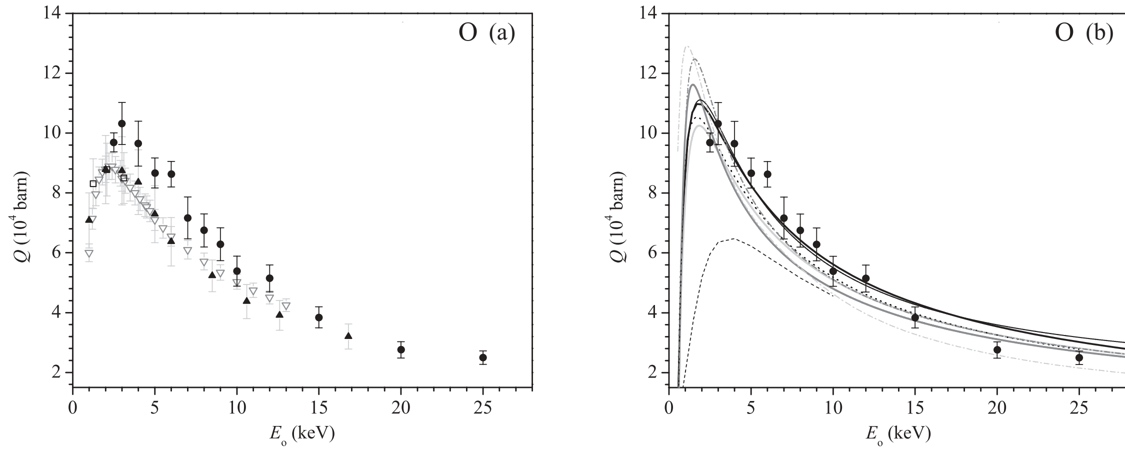


FIG. 6. Ionization cross section for oxygen as a function of electron energy $E_o$. (a) Comparison between experimental determinations. (b) Experimental data obtained in this work compared with theoretical and semiempirical approximations. Circles: this work; squares: Ref. [17]; gray open triangles: Ref. [20]; black open triangles: Ref. [21]; black thin solid line: Ref. [4]; light gray thick solid line: Ref. [9]; black thick solid line: Ref. [10]; black dashed line: Ref. [23]; black dotted line: Ref. [24]; light gray dash dotted line: Ref. [25]; dark gray thick solid line: Ref. [27]; and dark gray dash dotted line: Ref. [28].

Burr [44] were used. In the case of the expression published by Talukder *et al*. [28], alternative coefficients were recommended by one of the authors [45]. Campos *et al*. [10] obtained analytical functions for the five elements reported in this work by fitting theoretical data calculated by Segui *et al*. [5] based on DWBA. Bote *et al*. [4] determined analytical functions from the parametrization of theoretical calculations, performed by the former authors combining DWBA and PWBA.

The experimental data sets were taken from Hink and Paschke [22] for carbon, Tawara *et al*. [21] for carbon and oxygen, Glupe and Mehlhorn [20] for oxygen, Hink and Ziegler [15] for aluminum, Platten *et al*. [17] for silicon and oxygen, Shchagin *et al*. [16] for silicon, Jessenberger and Hink [18], and He *et al*. [19] for titanium. These results can be found in the compilation of the experimental data performed by Liu *et al*. [12], up to December, 1999. In the case of titanium, experimental determinations published by An *et al*. [11] in 2003 were also included.

Most of the data for carbon follow a similar trend (Fig. 5), except for the theoretical curve based on PWBA from Barlett and Stelbovics [23] that is far below. On the other hand, the experimental data from Hink and Paschke [22] show a severe overestimation at energies lower than 7 keV.

It is important to note that the values for carbon from this work (filled circles) were determined from the carbon planchets (bulk samples) and matrix corrections were applied [14]. The results agree with most of the data in the literature, which indicates that the matrix corrections implemented in the software POEMA are adequate.

For oxygen [Fig. 6(b)] the theoretical curve from Barlett and Stelbovics [23] is well below the other data. The improvements on PWBA from Tiwari and Tomar [24] and from Khare *et al*.

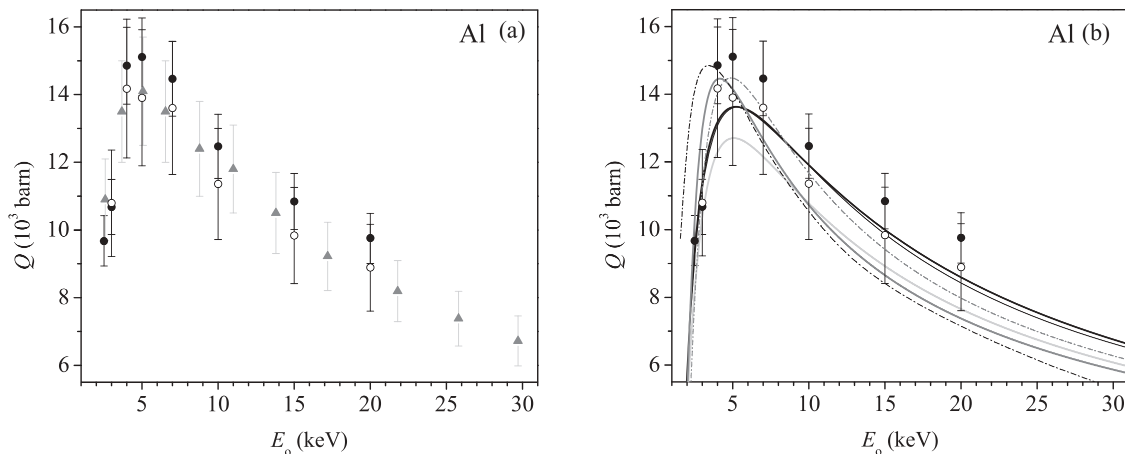


FIG. 7. Ionization cross section for aluminum as a function of the electron energy $E_o$. (a) Comparison between experimental determinations. (b) Experimental data obtained in this work compared with theoretical and semiempirical approximations. Circles indicate the results from the present work. Solid circles: Al film; open circles: $Al_2O_3$ film; triangles: Ref. [15]; black thin solid line: Ref. [4]; light gray solid line: Ref. [9]; black thick solid line: Ref. [10]; light gray dash dotted line: Ref. [25]; dark gray solid line: Ref. [27]; and dark gray dash dotted line: Ref. [28].

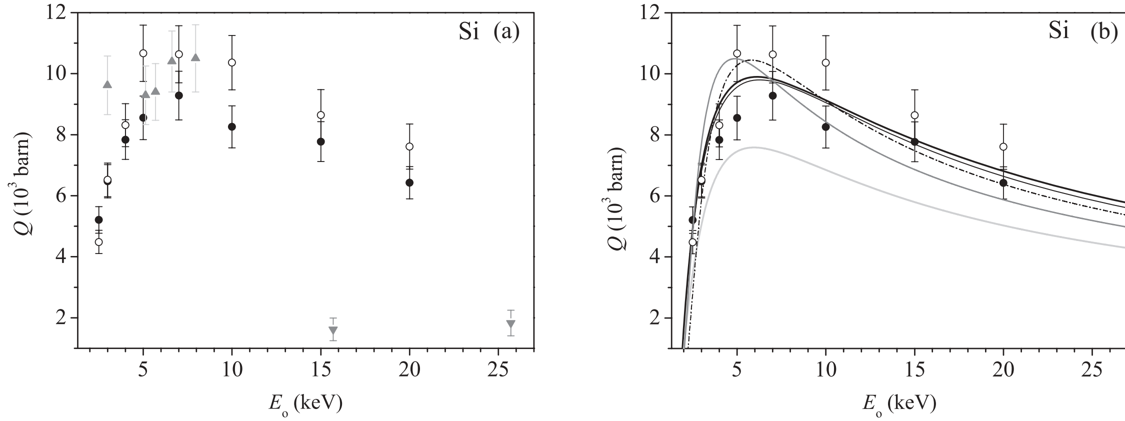


FIG. 8. Ionization cross section for silicon as a function of the electron energy $E_o$. (a) Comparison between experimental determinations. (b) Experimental data obtained in this work compared with theoretical and semiempirical approximations. Circles indicate the results from the present work. Solid circles: Si film; open circles: $SiO_2$; triangles: Ref. [16]; squares: Ref. [17]; black thin solid line: Ref. [4]; light gray solid line: Ref. [9]; black thick solid line: Ref. [10]; dark gray solid line: Ref. [27]; and dash dotted line: Ref. [28].

[25] give curves that agree better with the general trend. The experimental data sets from Platten *et al.* [17], Glupe and Mehlhorn [20], and Tawara *et al.* [21] lie well below the data obtained here and may have been affected by the older detector technology. The semiempirical curve from Campos *et al.* [10] based on DWBA shows the best agreement with our data.

For aluminum, silicon, and titanium most of the theoretical and semiempirical curves do not agree with the measured data at high overvoltages. The expression given by Hombourger [9] underestimates the global trend for aluminum [Fig. 7(b)] and silicon [Fig. 8(b)], whereas it is closer to the other determinations for titanium [Fig. 9(b)]. The values obtained in this work agree with the experimental results obtained by most of the other authors, except with the very low values published by Shchagin *et al.* [16] for silicon [Fig. 8(a)] and by He *et al.* [19] for titanium [Fig. 9(a)], which are systematically below all other determinations. An *et al.* [11] proposed that the underestimation for titanium could be due to errors in the thickness determination by He *et al.* [19], which consisted in weighing a known area of the material with a precision balance.

The theoretical model that agrees best with our experimental data is the DWBA formalism [4,10], that takes into account distortion and exchange effects. All experimental results obtained here seem to corroborate this theoretical approach.

The numerical average values $\bar{Q}_j$ of the cross sections obtained from the different samples in this work are presented in Table III. The errors were estimated as half of the maximum absolute difference between the ionization cross sections for each element.

Among the sources of error mentioned in Eq. (7) for aluminum, silicon, and titanium, the greatest influences correspond to the uncertainties associated with the solid angle subtended by the x-ray detector (6%) and to the uncertainties in the film linear thicknesses (10%, 17%, 4%, 7%, 9%, and 5% for Al, $Al_2O_3$, Si, $SiO_2$, Ti, and $TiO_2$, respectively); thus, the error associated with the experimental determinations is between 7% and 18%.

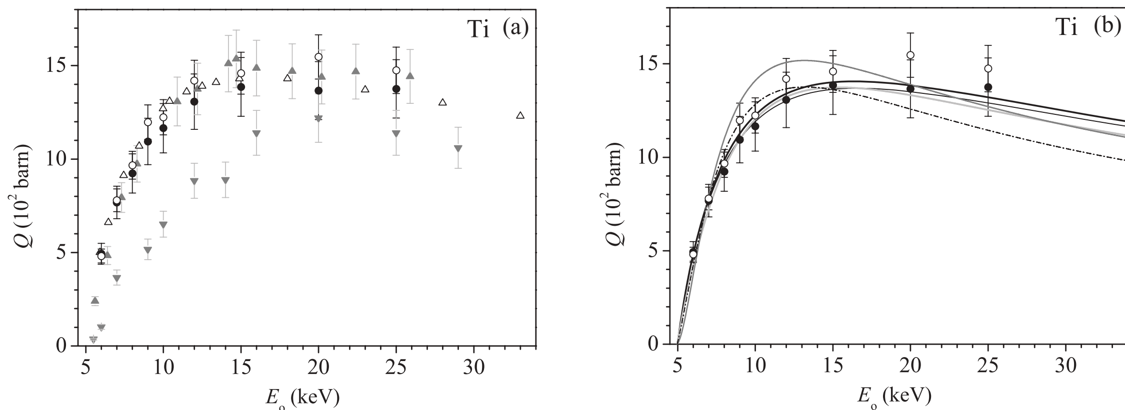


FIG. 9. $K$-shell ionization cross section for titanium as a function of the electron energy $E_o$. (a) Comparison between experimental determinations. (b) Experimental data obtained in this work compared with theoretical and semiempirical approximations. Circles indicate the results from the present work. Solid circles: Ti; open circles: $TiO_2$; solid up triangles: Ref. [11]; solid down triangles: Ref. [19]; open up triangles: Ref. [18]; black thin solid line: Ref. [4]; light gray solid line: Ref. [9]; black thick solid line: Ref. [10]; dark gray solid line: Ref. [27]; and dash dotted line: Ref. [28].

TABLE III. $K$-shell ionization cross sections and related absolute errors for C, O, Al, Si, and Ti as a function of the beam energy $E_o$.

| | $K$-shell ionization cross section $\bar{Q}_j$ ($10^3$ barn) | | | | |
|---|---|---|---|---|---|
| $E_o$ (keV) | C | O | Al | Si | Ti |
| 2.5 | 280 ± 40 | 97 ± 7 | 9.7 ± 0.4 | 4.8 ± 0.3 | |
| 3 | 260 ± 40 | 104 ± 7 | 10.65 ± 0.05 | 6.59 ± 0.05 | |
| 4 | 230 ± 40 | 97 ± 2 | 14.5 ± 0.4 | 8.1 ± 0.3 | |
| 5 | 200 ± 20 | 86 ± 2 | 14.6 ± 0.7 | 9.5 ± 1.0 | |
| 6 | 171 ± 9 | 90 ± 10 | | | 0.485 ± 0.005 |
| 7 | 152 ± 9 | 71 ± 2 | 14.1 ± 0.5 | 9.9 ± 0.7 | 0.773 ± 0.005 |
| 8 | 140 ± 10 | 67 ± 5 | | | 0.95 ± 0.02 |
| 9 | 124 ± 9 | 62 ± 5 | | | 1.15 ± 0.05 |
| 10 | 110 ± 10 | 54 ± 3 | 12.0 ± 0.6 | 9 ± 1 | 1.20 ± 0.02 |
| 12 | 97 ± 4 | 51 ± 4 | | | 1.37 ± 0.05 |
| 15 | 76 ± 5 | 38 ± 2 | 10.5 ± 0.6 | 8.2 ± 0.5 | 1.43 ± 0.04 |
| 20 | 53 ± 4 | 28 ± 3 | 9.4 ± 0.5 | 6.9 ± 0.6 | 1.50 ± 0.09 |
| 25 | 39 ± 3 | 25 ± 2 | | | 1.43 ± 0.05 |

For carbon (Fig. 5) and oxygen (Fig. 6), the uncertainty of the detector efficiency (estimated to be 8% for O and 10% for C) has to be added to the other two sources of error, resulting in uncertainties between 12% and 22% for the individual determinations.

The ionization cross sections of aluminum calculated from the emission spectra of Al and $Al_2O_3$ films are indistinguishable within the experimental uncertainty (Fig. 7). In the case of Si and $SiO_2$ the discrepancies are slightly higher (Fig. 8). The experimental data presented here for silicon extend the energy range from 2.5 to 20 keV, while all experimental data available in the literature were limited to the range of 3–8 keV. The cross sections obtained from the Ti and $TiO_2$ films (Fig. 9) show similar values, in the same way as in Al and $Al_2O_3$ films. Considering that the innermost atomic shells are little affected by the chemical environment, only small differences between the $K$-shell ionization cross sections of native and oxidized elements were expected. Any effect caused by chemical bonding is obliterated by the experimental uncertainty.

The experimental data in the literature show a wide dispersion for the elements in the studied energy range. It is not straightforward to assess the quality of these data, considering that in older experiments oxidation layers were not visible with detectors with thick windows. In addition, the use of nominal values for the detector acceptance solid angle may have induced significant deviations from the true ionization cross sections.

## VI. CONCLUSION

The experimental values for cross sections for $K$-shell ionization by electron impact for C, O, Al, Si, and Ti obtained in this work for electron incident energies between 2.5 and 25 keV are consistent with data obtained by other authors. In this work a clear estimate of the different sources of error involved in the acquisition process was obtained. The main errors come from

(i) The solid angle subtended by the x-ray detector, usually overestimated when calculated by geometrical means. In this work it was determined indirectly with Monte Carlo simulated bremsstrahlung, reducing the error significantly.

(ii) The presence of a native oxidation layer on the elemental films. In this work this layer had its thickness calculated with the aid of the O-$K$ peak and its effects were introduced in the spectral processing procedure.

(iii) The film thickness and density. In this work they were determined with XRR performed on large area films on Si substrates. The error associated with this data might be further reduced taking the oxide layer into account and simulating multilayer internal reflections in the processing of the reflectograms.

(iv) The detector intrinsic efficiency which is difficult to estimate in the energy range between 0.25 and 0.6 keV. In this work, a 300-nm polymer, a 30-nm aluminum, and a 100-nm dead layer were taken into account. To reduce these errors, the layer thicknesses and the absorption coefficients of the low-energy x rays in the detector materials would have to be better known.

The comparison of our experimental data with theoretical and semiempirical formulas showed that the trend of the measured data is best represented by the DWBA model. In the case of oxygen, the experimental data presented here shows a better agreement with the DWBA calculations than all other experimental data sets, which are systematically below the DWBA curve. Particularly for silicon, the experimental ionization cross sections were obtained in a broad range of energies, establishing a data set that corroborates the theoretical and semiempirical curves.

Comparing the data obtained in the present work for silicon and titanium with the experimental data available in the literature, it becomes clear that some sets of ionization cross sections present a high level of inaccuracy. The scarcity and spread of the data make it difficult to decide among the theoretical approaches that should be followed. The improvements due to the film fabrication in ultrahigh vacuum and the use of an efficient SDD-EDX detector, with ultrathin window, able to detect the native oxide on thin film surfaces and a careful spectral processing, allowed us to obtain data that can reliably support a theoretical model.

## ACKNOWLEDGMENTS

This work was partially supported by the Asociación de Universidades Grupo Montevideo (AUGM), the Consejo Nacional de Investigaciones Científicas y Técnicas (CONICET) of Argentina, and the Coordenação de Aperfeiçoamento de Pessoal de Nível Superior (CAPES), the Conselho Nacional de desenvolvimento Científico e Tecnológico (CNPq), and the Fundação de Amparo à Pesquisa do Estado do Rio Grande do Sul (FAPERGS) of Brazil.



[1] D. Ze-Jun and Wu Ziqin, J. Phys. D **27**, 387 (1994).

[2] C. J. Powell, A. Jablonski, W. S. M. Werner, and W. Smekal, Appl. Surf. Sci. **239**, 470 (2005).

[3] M. Inokuti, Rev. Mod. Phys. **43**, 297 (1971).

[4] D. Bote, F. Salvat, A. Jablonski, and C. Powel, At. Data Nucl. Data Tables **95**, 871 (2009).

[5] S. Segui, M. Dingfelder, and F. Salvat, Phys. Rev. A **67**, 062710 (2003).

[6] J. Eichler, *Lectures on Ion-Atom Collisions: From Nonrelativistic to Relativistic Velocities,* 1st ed. (Elsevier, Amsterdam, 2005).

[7] M. Green and V. Cosslett, Proc. Phys. Soc. London **78**, 1206 (1961).

[8] C. Quarles, Phys. Rev. A **13**, 1278 (1975).

[9] C. Hombourger, J. Phys. B **31**, 3693 (1998).

[10] C. Campos, M. A. Z. Vasconcellos, J. Trincavelli, and S. Segui, J. Phys. B **40**, 3835 (2007).

[11] Z. An, M. Liu, Y. Fu, Z. Luo, C. Tang, C. Li, B. Zhang, and Y. Tang, Nucl. Instrum. Methods Phys. Res., Sect. B **207**, 268 (2003).

[12] M. Liu, Z. An, C. Tang, Z. Luo, X. Peng, and X. Long, At. Data Nucl. Data Tables **76**, 213 (2000).

[13] D. Joy, *A Database of Electron-Solid Interactions*, http://web.utk.edu/~srcutk/htm/interact.htm (2008).

[14] R. Bonetto, G. Castellano, and J. Trincavelli, X-Ray Spectrom. **30**, 313 (2001).

[15] W. Hink and A. Ziegler, Z. Phys. **269**, 222 (1969).

[16] A. Shchagin, V. Pristupa, and N. Khizhnyak, Nucl. Instrum. Methods Phys. Res., Sect. B **84**, 9 (1994).

[17] H. Platten, G. Schiwietz, and G. Nolte, Phys. Lett. A **107**, 83 (1985).

[18] J. Jessenberger and W. Hink, Z. Phys. A **275**, 331 (1975).

[19] F. He, F. Peng, X. Long, Z. Luo, and Z. An, Nucl. Instrum. Methods Phys. Res., Sect. B **129**, 445 (1997).

[20] G. Glupe and W. Mehlhorn, Phys. Lett. A **25**, 274 (1967), and references therein.

[21] H. Tawara, K. Harrison, and F. De Heer, Physica **63**, 351 (1973).

[22] W. Hink and H. Paschke, Phys. Rev. A **4**, 507 (1971).

[23] P. Barlett and A. Stelbovics, At. Data Nucl. Data Tables **86**, 235 (2004).

[24] N. Tiwari and S. Tomar, J. At. Mol. Sci. **2**, 109 (2011).

[25] S. P. Khare, V. Saksena, and J. M. Wadehra, Phys. Rev. A **48**, 1209 (1993).

[26] J. Santos, F. Parente, and Y. Kim, J. Phys. B **36**, 4211 (2003).

[27] A. K. F. Haque, M. A. Uddin, A. K. Basak, K. R. Karim, and B. C. Saha, Phys. Rev. A **73**, 012708 (2006).

[28] M. Talukder, S. Bose, and S. Takamura, Int. J. Mass Spectrom. **269**, 118 (2008).

[29] M. Birkholz, *Thin Film Analysis by X-ray Scattering* (Wiley-VCH, Berlin, 2006).

[30] J. Trincavelli and G. Castellano, Spectrochim. Acta, Part B **63**, 1 (2008).

[31] C. Visñovezky, S. Limandri, M. E. Canafoglia, R. Bonetto, and J. Trincavelli, Spectrochim. Acta, Part B **62**, 492 (2007).

[32] S. Limandri, A. Carreras, and J. Trincavelli, Microsc. Microanal. **16**, 583 (2010).

[33] S. Limandri, Ph.D. thesis, Universidad Nacional de Córdoba, Argentina, 2011, http://www.famaf.unc.edu.ar/publicaciones/documents/serie_d/DFis150.pdf.

[34] J. Bearden, Rev. Mod. Phys. **39**, 78 (1967).

[35] S. Reed, J. Phys. E **5**, 997 (1972).

[36] G. Knoll, *Radiation Detection and Measurement,* 3rd ed. (John Wiley & Sons, New York, 2000), p. 634.

[37] M. Pia, P. Saracco, and M. Sudhakar, IEEE Trans. Nucl. Sci. **56**, 3650 (2009).

[38] F. Salvat, J. M. Fernández-Varea, and J. Sempau, in *Proceedings of the OECD/NEA Data Bank, Issy-les-Moulineaux, France* (OECD Publication, Paris, France, 2003), http://www.oecd-nea.org/general/mnb/2003/october.html.

[39] S. Perkins, D. Cullen, M. Chen, J. Hubbell, J. Rathkopf, and J. Scofield, Lawrence Livermore National Laboratory Report No. UCRL-50400, Vol. 30, 1991.

[40] J. H. Hubbell, P. N. Trehan, N. Singh, B. Chand, D. Mehta, M. L. GargL, R. R. Garg, S. Singh, and S. Puri, J. Phys. Chem. Ref. Data **23**, 339 (1994).

[41] C. T. Chantler, J. Phys. Chem. Ref. Data **24**, 71 (1995).

[42] H. M. Choi, S.K. Choi, O. Anderson, and K. Bange, Thin Solid Films **358**, 202 (2000).

[43] K. Bell, H. Gilbody, A. Hughes, A. Kingston, and F. Smith, J. Phys. Chem. Ref. Data **12**, 891 (1983).

[44] J. Bearden and A. Burr, Rev. Mod. Phys. **39**, 125 (1967).

[45] M. Talukder (private communication).